2-22-2010

Relation between Ga ordering and magnetostriction of Fe-Ga alloys studied by x-ray diffuse scattering

Y. Du
Iowa State University

Mianliang Huang
Iowa State University

S. Chang
Iowa State University

Deborah L. Schlagel
Iowa State University, schlagel@iastate.edu

Thomas A. Lograsso
Iowa State University, lograsso@ameslab.gov

Follow this and additional works at: http://lib.dr.iastate.edu/ameslab_pubs

See next page for additional authors

Part of the Condensed Matter Physics Commons, and the Metallurgy Commons

The complete bibliographic information for this item can be found at http://lib.dr.iastate.edu/ameslab_pubs/68. For information on how to cite this item, please visit http://lib.dr.iastate.edu/howtocite.html.

Relation between Ga ordering and magnetostriction of Fe-Ga alloys studied by x-ray diffuse scattering

Abstract

Transmission synchrotron diffraction was employed to characterize the Ga ordering in magnetostrictive $Fe_{100-x}Ga_x$ alloys with Ga concentrations from 0 to 20.3 at. %. The experiments focused on the development of atomic short-range ordering (SRO) by analysis of the diffuse scattering appearing at superlattice positions of the $D0_3$ ordered alloy structure. No SRO was found for Ga concentrations less than 4 at. %. Between 13 and 20.3 at. %, $D0_3$-type SRO clusters are observed whose size increases with Ga concentration for both slow-cooled and quenched samples. Thermal quenching of the samples suppresses the cluster sizes when compared to slow-cooled samples of the same concentration. For quenched samples with large Ga concentration, Ga pairing is evidenced by growing B2-type correlations. At low concentrations, the presence of SRO appears to have little (if any) effect on the enhanced magnetostriction. However, the dramatic suppression of magnetostriction near ~20 at. % Ga can be linked rapid growth of SRO just before the onset of long-range chemical order.

Authors

Y. Du, Mianliang Huang, S. Chang, Deborah L. Schlagel, Thomas A. Lograsso, and Robert J. McQueeney

Relation between Ga ordering and magnetostriction of Fe-Ga alloys studied by x-ray diffuse scattering

Y. Du,[1,2] M. Huang,[2] S. Chang,[2,*] D. L. Schlagel,[2] T. A. Lograsso,[2] and R. J. McQueeney[1,2]

[1]*Department of Physics and Astronomy, Iowa State University, Ames, Iowa 50011, USA*

[2]*Division of Materials Sciences and Engineering, Ames Laboratory, Ames, Iowa 50011, USA*

Transmission synchrotron diffraction was employed to characterize the Ga ordering in magnetostrictive $Fe_{100-x}Ga_x$ alloys with Ga concentrations from 0 to 20.3 at. %. The experiments focused on the development of atomic short-range ordering (SRO) by analysis of the diffuse scattering appearing at superlattice positions of the $D0_3$ ordered alloy structure. No SRO was found for Ga concentrations less than 4 at. %. Between 13 and 20.3 at. %, $D0_3$-type SRO clusters are observed whose size increases with Ga concentration for both slow-cooled and quenched samples. Thermal quenching of the samples suppresses the cluster sizes when compared to slow-cooled samples of the same concentration. For quenched samples with large Ga concentration, Ga pairing is evidenced by growing B2-type correlations. At low concentrations, the presence of SRO appears to have little (if any) effect on the enhanced magnetostriction. However, the dramatic suppression of magnetostriction near ~20 at. % Ga can be linked rapid growth of SRO just before the onset of long-range chemical order.

I. INTRODUCTION

Magnetostrictive materials are widely used in making electronic parts such as actuators and sensors. However, materials with large magnetostriction (MS), such as Terfenol-D, are both brittle and expensive, which limits their application. The addition of Ga to α-Fe greatly enhances the saturation MS along [100] direction up to tenfold.[1] Moreover, Fe-Ga alloys exhibit superior mechanical properties compared to other materials with large MS.[1] Although the maximum magnetostrictive strain of Fe-Ga is not the largest compared to other magnetostrictive materials, Fe-Ga is still a promising functional material with enhanced MS because of its good mechanical properties. The origin of enhanced MS in Fe-Ga is unclear despite the fact that significant efforts have been made to understand it. Wu *et al.*[2,3] suggested that the enhanced MS was related to local ordering of Ga atoms; the B2 structure which gave rise to the pairing of Ga atoms played a positive role while the $D0_3$ structure was determined to be detrimental to MS. On the other hand, Khachaturyan and Viehland[4,5] suggested that reorientation within tetragonal nanoclusters in Fe-Ga resulted in the enhanced MS.

MS is usually expressed by the magnetostrictive coefficient λ. From Kittel,[6] the saturated MS along [100] direction (tetragonal MS) can be expressed by

$$\frac{3}{2}\lambda_{100} = -\frac{b_1}{2c'},$$

where b_1 is magnetoelastic coupling factor and c' is tetragonal shear modulus.

Figure 1 shows the dependence of MS on Ga concentration.[7] Based on the work of Xing *et al.*, the magnetostrictive behavior is separated into four regions. In region I, MS increases monotonously with concentration and reaches the first maximum at about 18–20 at. % Ga depending on heat treatment. A gradual softening of the shear modulus with Ga concentration is reported to occur up to 27 at. %

Ga and the second peak appearing at about 27 at. % Ga (between regions III and IV) has been attributed to the minimum of the shear modulus since there is no corresponding maximum with magnetoelastic coupling factor.[8,9]

While the shear-modulus softening also explains, in part, the general increase in the MS in region I, it cannot account for the existence of the first MS peak occurring between regions I and II. The first peak may result from an unusual or nonmonotonic evolution of the magnetoelastic coupling factor with Ga concentration. Comparison of the MS to the metastable phase diagram shown in Fig. 2 serves as a guide to the behavior of the MS in Fe-Ga alloys. The first MS peak occurs close to the transformation from a disordered alloy with A2 structure, to an ordered alloy with $D0_3$ structure. This provides a clue that details of the Ga chemical ordering play some role in the enhanced MS. In particular, the sensi-
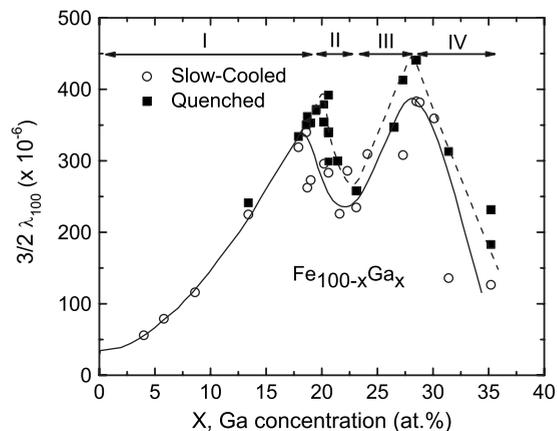

FIG. 1. Saturated MS for quenched (filled squares) and slow-cooled Fe-Ga (circles) along [100] direction verses Ga concentration. Solid and dashed lines are guide to the eyes for slow-cooled and quenched MS curves, respectively. Different regions of MS behavior (I, II, III, and IV) are described in the text. From Ref. 7.
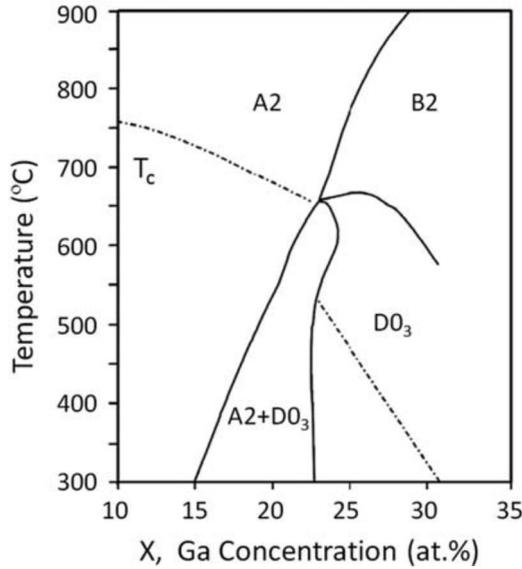
FIG. 2. Metastable phase diagram for Fe-Ga alloys (Ref. 10). Solid lines describe solid-solid phase transformations between the A2, B2, and D0$_3$ ordered alloy phases. The dash-dotted line indicates the ferromagnetic ordering (Curie) temperature.

tivity of MS to heat treatment, most notably the retention of large MS by quenching, indicates that MS is maximized in the A2 phase, where Ga atoms form short-range ordering (SRO).

The occurrence of SRO in the Fe-Ga alloys in region I was clearly shown by the synchrotron diffraction work of Xing *et al.*,[7] and later by the neutron-diffraction work of Cao *et al.*[11] However, the SRO has not been fully characterized in previous structural studies. An Fe$_{80}$Ga$_{20}$ sample prepared by blade milling of arc-melted alloy was reported to be completely disordered from Mössbauer spectroscopy results[12] while the Fe-Ga alloys were claimed to have some degree of Ga SRO in another Mössbauer investigation of the Fe-Ga prepared by rapid solidification.[13] Transmission electron microscopy (TEM),[10] neutron diffraction,[11,14] and conventional x-ray diffraction[15,16] studies did not report the presence of the SRO in the single crystals of Fe-Ga alloys prepared via water quenching or rapid solidification. In conventional x-ray diffraction studies, SRO is difficult to quantitatively characterize because of the extremely weak peak intensity of the SRO diffuse scattering due to the close x-ray atomic factors between Fe and Ga atoms. However, high-energy x-ray diffraction performed at a synchrotron source with sufficient flux can be used to characterize the SRO in the Fe-Ga alloys.[7] Furthermore, the high-energy x-ray fully penetrates the sample volume and therefore reveals the bulk structural properties of the alloys.

In this work, we systematically investigated the SRO in Fe-Ga alloys with a concentration range from 0 to 20.3 at. % Ga quantitatively using high-energy x-ray diffraction. The Ga ordering is characterized around the boundary between region I and region II in order to determine the role that Ga atomic ordering plays in MS. Comparison is also made for some alloys at both slow-cooled and water-quenched conditions because of the importance of the thermal history on MS in Fe-Ga alloys as shown in Fig. 1. Results show that D0$_3$-type SRO peaks have appeared when Ga concentrations are as low as 13 at. %. The presence of D0$_3$ SRO in samples with low Ga concentrations plays little (if any) effect on MS. However, MS is suppressed when the size of SRO experiences a dramatic increase and reaches certain value in samples with ~18–20 at. % Ga concentrations depending on different thermal histories.

II. EXPERIMENT

A. Sample preparation

Gallium (99.999 wt % pure) and electrolytic iron (99.99 wt % pure) were cleaned and arc melted together several times under an argon atmosphere. To prepare single-crystal samples, the as-cast ingot was placed in an alumina crucible and heated under a vacuum to 1500 °C. After reaching 1500 °C, the growth chamber was backfilled with ultrahigh-purity argon to a pressure of 2.76×10^5 Pa. Following pressurization, heating was continued until the ingot reached a temperature of 1600 °C and held for 1 h before being withdrawn from the furnace at a rate of 5 mm/hr. Following crystal growth, the ingot was annealed at 1000 °C for 168 h (using heating and cooling rates of 10 °C/min). Small parallelepipeds (5 mm × 5 mm × 0.5 mm) were cut from the ingot by wire electrical discharge machining with either [001] or [110] direction normal to the surface. Some samples were sealed in a quartz tube filled with high-purity argon and annealed at 1000 °C for 4 h then quenched by water. Sample orientation was determined by backreflection Laue diffraction to within ±0.25° of the desired orientation. Oriented samples were then prepared using standard metallographic procedures with the final polishing step using diamond paste, followed by a Nital etch. Concentration measurements were done with energy-dispersive spectrometers in a JEOL 840A scanning electron microscope, using Fe and Ga standards for calibration.

B. X-ray diffuse-scattering measurements

The metastable phase diagram in Fig. 2 indicates that three different crystallographic phases may appear in our samples; A2 is a disordered bcc structure with Ga distributed randomly, B2 is a simple cubic structure (CsCl structure) with Fe or Ga occupying the center position of the bcc structure at random, and D0$_3$ is related to the B2 structure but now the Ga only randomly occupies the center of alternating cubes. The resulting larger unit cell is fcc based. These structures are schematically shown in Fig. 3.

To search for evidence of SRO/LRO (long-range ordering) alloy structures, review of the diffraction conditions for each structure type is useful. The A2 structure has the same Bragg condition as the bcc structure: $h+k+l$=even, where h, k, and l are Miller indices. For a cubic structure, Miller indices are defined as

$$\vec{q} = \frac{2\pi}{a}(h \cdot \hat{i} + k \cdot \hat{j} + l \cdot \hat{k}),$$

where $\vec{q}$ is the vector in reciprocal space and a is cubic lattice constant. The simple cubic B2 structure allows all integers h,
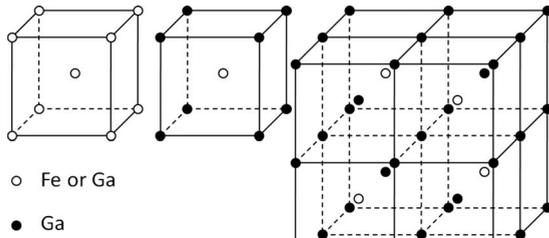
FIG. 3. Crystal structures for (left) A2, (center) B2, and (right) D0$_3$ structures of Fe$_{100-x}$Ga$_x$ alloys.

k, and l. The D0$_3$ arrangement of Ga atoms can be represented as an fcc structure with a doubled unit cell. The Bragg condition for fcc structure is h, k, and l are all even or odd. Due to the doubling of the unit cell in the D0$_3$ structure, the peak condition is: $2h$, $2k$, and $2l$ are all even or odd where h, k, and l refer to the original cubic cell of bcc. Table I shows the first few allowed peaks for each type of chemical ordering.

For the remainder of the paper, we refer to the diffraction peaks stemming from the parent A2 structure as fundamental Bragg peaks, as these are very strong peaks arising from the average bcc structure and occur in each ordered/disordered structure. The additional weak peaks resulting from Ga ordering in either the B2 or D0$_3$ structure are referred to as superlattice peaks. In the region of the phase diagram approximately below and left of the first maximum in the MS, it is expected that Ga ordering is short ranged. In this case, instead of the sharp and narrow superlattice peaks, we expect broad and diffuse intensity arising from SRO at the superlattice position. Diffuse SRO peaks observed in reciprocal space are indicative of arrangement of Ga within the SRO regions which we expect to be either B2 or D0$_3$ in character.

Experiments were performed in sector 6 station D (6ID-D), μ-CAT, Advanced Photon Source (APS), Argonne National Laboratory, using 99.6 KeV x-rays. Single-crystal samples were mounted to the center of a 6-circle diffractometer. Due to the high-energy x-ray beam, scattering angles were typically below 10° and experiments were performed in transmission geometry. Given the sample thickness of

TABLE I. Three different structures and their corresponding peak conditions. "✓" indicates that a reflection is observed in the given structure while "X" indicates that it is forbidden by symmetry. Reflections appearing in all three alloy structure types are labeled as fundamental peaks. Those appearing only weakly due to ordering are called superlattice peaks.

Reflection condition (HKL)	A2	B2	D0$_3$
(0.5 0.5 0)	X	X	X
(0.5 0.5 0.5) (superlattice)	X	X	✓
(100) (superlattice)	X	✓	✓
(110) (fundamental)	✓	✓	✓
(111) (superlattice)	X	✓	✓
(200) (fundamental)	✓	✓	✓

~0.5 mm and the lateral extent of the beam size of ~0.5 mm, the beam will sample thousands of magnetic domains with characteristic size of order 10 μm. We employed two different detectors for our measurements. (1) To get an overview of the diffuse-scattering features, a Mar 345 image plate detector was used. The distance between sample and detector was 961.6 mm. The samples were aligned with the incident x-ray beam along either the [011] or [001] crystallographic directions. Based on this geometry, the surveys of reciprocal space on the Ewald sphere was tangential to either the (HLL) or ($HK0$) plane, respectively. Figure 4(a) shows the result obtained with the image plate detector for slow-cooled Fe$_{81.7}$Ga$_{18.3}$ and indicates typical diffuse-scattering features to be discussed below. (2) For quantitative scans of the diffuse intensity in well-defined symmetry directions, a Canberra germanium point detector was used. To reduce the background, an energy window of ~2 keV was defined at the nominal energy for elastic scattering so that most of inelastic contributions, such as Compton scattering, were not counted. Several line scans in reciprocal space were repeated for each concentration and heat treatment. Scans were made along various directions in the [HLL] plane through various peak positions corresponding to A2, B2, and/or D0$_3$ Bragg positions. The counts of the detector were normalized to the corresponding x-ray flux measured by a beam monitor.

III. RESULTS

Now, we will describe the general features contained in the diffuse scattering. In Fig. 4(a), the round features appearing at superlattice positions such as (100) (D0$_3$ or B2) and (0.5 0.5 0.5) (D0$_3$) are SRO peaks. The SRO peaks are observed at other symmetry equivalent positions throughout the [HLL] plane, although the signal gets weaker for higher-order indices. The weaker signal is due to the sampling of scattering on the Ewald sphere, as higher-order index positions are further from the actual [HLL] symmetry plane. The irregularly shaped (elongated or butterfly shaped) features appearing in the vicinity of fundamental Bragg positions are thermal diffuse-scattering (TDS) peaks. TDS arises from phonon scattering and is only weakly affected by chemical SRO, as will be discussed below. Finally, the rings of scattering are due to a small volume fraction of polycrystalline alloy on the surface of the samples. The amount of polycrystalline alloy, formed during surface polishing, was reduced by acid etching, as described in the sample preparation. Other contributions to the diffuse scattering are possible in an alloy, such as Huang scattering due to long-range strains. However, this is usually only important near the fundamental Bragg positions and will not be considered further.

We now turn to the line scans performed in the symmetry plane. Figure 4(a) illustrates the two reciprocal space scan directions that cut through the SRO diffuse scattering, as shown in Figs. 4(b)–4(e). Figures 4(b) and 4(c) show data for quenched samples while Figs. 4(d) and 4(e) show data for slow-cooled samples with corresponding concentrations indicated in the figures. The estimated background (shown as a hatched region) was determined from scans performed without a sample and arises mainly from air scattering, which will be described below.
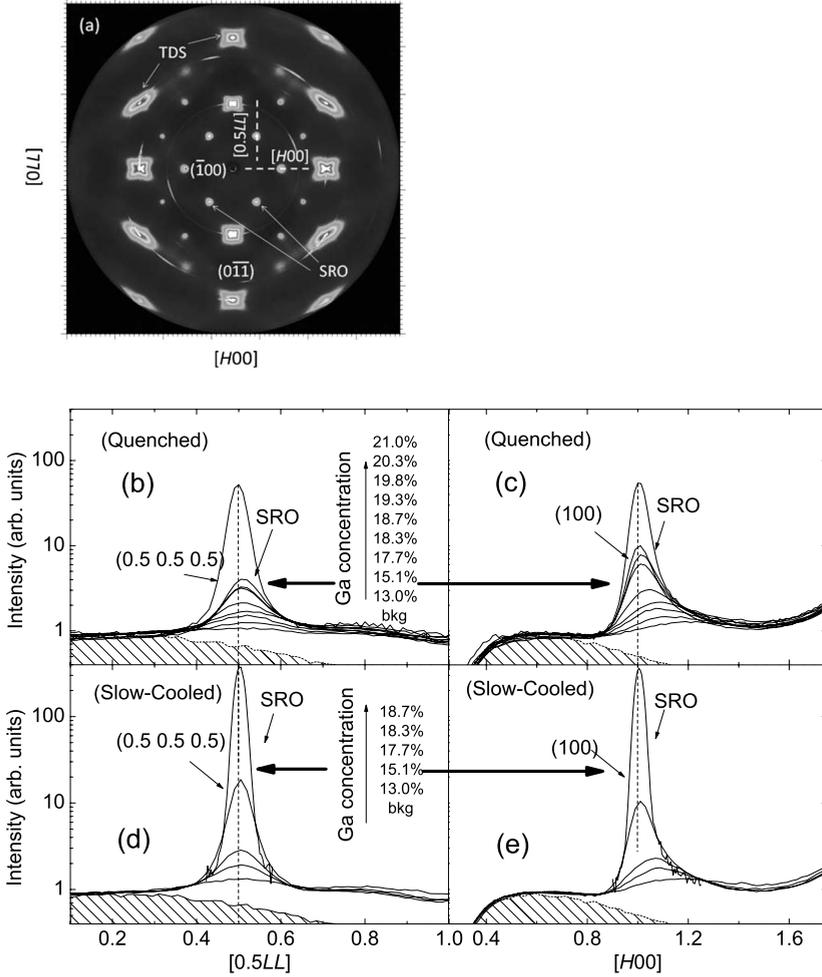
FIG. 4. (a) Image of x-ray diffuse scattering using Mar 345 image plate from a single crystal of slow-cooled $Fe_{81.7}Ga_{18.3}$ with [011] direction aligned along the incident x-ray beam. Diffuse features are labeled as either originating from SRO or thermal diffuse scattering, as described in the text. Linear scans measured along [0.5LL] direction are shown in (b) (quenched) and (d) (slow cooled). Linear scans along [H00] are shown in (c) (quenched) and (e) (slow cooled). Linear scans are measured using a Canberra germanium point detector and indicated as the dashed line in (a). The hatched region is the background.

Based on Figs. 4(b)–4(e), the general trends are: (I) for a given Ga concentration, slow-cooled samples have much more intense and narrower peaks than quenched ones; (II) for the same heat treatment, samples with higher Ga concentration have higher and narrower peaks; (III) the SRO peak positions deviate from their nominal position in reciprocal space, especially for (100) peaks where the peak position is as high as (1.2,0,0) for the lower Ga concentrations.

IV. DATA ANALYSIS

There are several components contributing to the data shown in Fig. 4. (I) The background due mainly to air scattering; (II) TDS from the thermal vibration of the atoms; (III) "Size-effect" scattering due to the bigger Ga atoms in the alloy pushing the Fe atoms away from the cubic lattice position; and (IV) SRO diffuse scattering due to clustering of solute atoms. Besides these four components, there are other contributions to the background such as Compton scattering. As mentioned before, an energy window was set to minimize most of the inelastic spectrum such as Compton scattering.

The observed background scattering arises primarily from small-angle air scattering of x rays from the direct beam. This becomes a serious issue at very small angles and is mitigated to some extent by the placement of a small tungsten beamstop behind the sample. This removes a significant

portion of the air scattering and nonscattered direct beam but limits the minimum attainable scattering angle. The remaining air scattering that bypasses the beamstop was measured by removing the samples. After considering the attenuation of the incident-beam intensity due to sample absorption, the measured air scattering was subtracted from the data.

The TDS of Fe-Ga is caused by thermal vibrations of the atoms and can be estimated by the TDS of α-Fe which is calculated based on the phonon dispersion of α-Fe.[17] Figure 5 shows an example of the calculated TDS compared to the normalized data (measured with background removed) along [1LL] direction in reciprocal space. The calculated results are useful for identifying features of the diffuse scattering that arise from thermal vibrations, as opposed to Ga ordering. However, the TDS calculations based on phonon models give only qualitative agreement with the data, therefore we ultimately used analytical functions to fit the TDS portion of the total scattering. The chosen analytical functions vary based on the type of reciprocal space scan that was performed. In defining these functions, we assume that the phonons do not change dramatically when Ga is substituted for Fe. This is true for most of the phonon branches with the exception of the transverse [110] phonons that are known to soften with the addition of Ga.[17]

Small static displacements of atoms from their nominal positions in an alloy are caused by size differences of the two
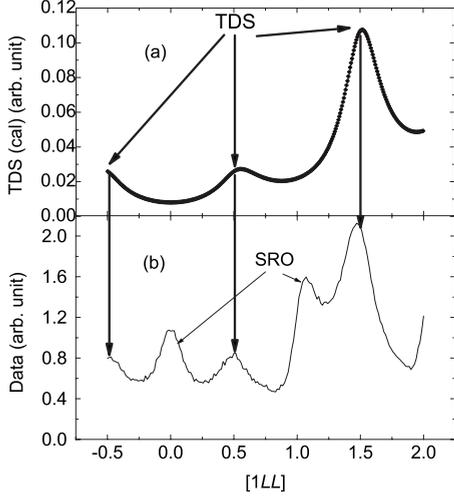
FIG. 5. Intensity of calculated TDS (a) obtained from a phonon model for α-Fe (Ref. 17) as compared to the normalized data (background removed) and (b) along $[1LL]$ direction for quenched $Fe_{82.3}Ga_{17.7}$ in reciprocal space. TDS peaks are indicated by bold arrows while SRO peaks are indicated by ordinary arrows.

species. Such displacements give rise to diffuse scattering called size-effect (SE) scattering, which is given by

$$\sum_{jj'} \beta_j^{i\vec{q}} \cdot \vec{r}_{jj'} \exp(i\vec{q} \cdot \vec{r}_{jj'}), \tag{1}$$

where β_j is size-effect parameter and defined as

$$\beta_j = \left(\frac{f_{Fe}}{f_{Ga} - f_{Fe}}\right) \left\{ -\left(\frac{p_{Fe}}{p_{Ga}} + \alpha_j\right) \varepsilon_{FeFe}^j + \left(\frac{p_{Ga}}{p_{Fe}} + \alpha_j\right) \right.$$
$$\left. \times \left(\frac{f_{Ga}}{f_{Fe}}\right) \varepsilon_{GaGa}^j \right\}, \tag{2}$$

where f is the atomic scattering factor; α is the short-range ordering parameter; ε_{AB} is the change from average distance for A-B pair; and p is the concentration of atom.[18] Since the size of Ga is larger than that of Fe, ε_{GaGa} is positive while ε_{FeFe} is negative. The sign of β is hence the same with that of $(f_{Ga} - f_{Fe})$, the difference in the atomic scattering factors of the two atoms. For our x-ray scattering experiment at 100 keV, $f_{Ga} > f_{Fe}$, leading to a positive value of β.

By limiting consequences of the size effect to nearest neighbors and next-nearest neighbors, formula (1) can be simplified. Formulas (3) and (4) give simplified fitting functions along $[0.5LL]$ and $[H00]$, respectively, and were used to fit the size-effect scattering,

$$I_{SE}^{0.5LL} = -2\pi\beta_1\{\cos(2\pi L) + 1\} - 8\pi\beta_2 L \sin(2\pi L), \tag{3}$$

$$I_{SE}^{H00} = -8\pi\beta_1 H \sin(\pi H) - 4\pi\beta_2 H \sin(2\pi H). \tag{4}$$

The size-effect scattering generally can give an asymmetric contribution in the vicinity of a peak in the SRO scattering and lead to a shift of the SRO peak from the nominal superlattice position, as observed here. However, as described below, our approach of using only the simplified formulas in Eqs. (3) and (4) cannot fully account for the peak shift. How-
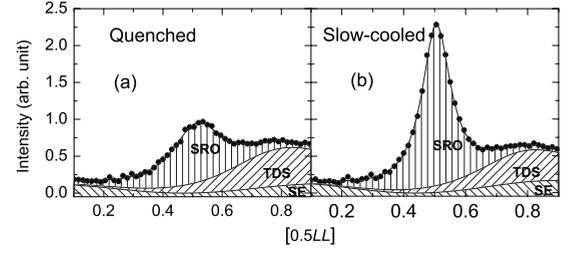

FIG. 6. Fitting of diffuse-scattering data from (a) quenched and (b) slow-cooled $Fe_{82.3}Ga_{17.7}$ along $[0.5LL]$. The dots correspond to the raw data with background removed. The hatched regions correspond to the contributions of SRO, TDS, and SE scattering to the total fit (solid line).

ever, accounting for this contribution leads to more reliable description of the SRO.

After accounting for background, TDS, and size-effect scattering, the remaining intensity is assumed to arise from SRO correlations of the atoms. The SRO diffuse-scattering peaks are fit with a Lorentzian function, which has the form of

$$I_{SRO} = \frac{2A}{\pi} \frac{w(\vec{q})}{4|\vec{q} - \vec{q}_0|^2 + w^2(\vec{q})}, \tag{5}$$

where $w(\vec{q})$ is the full width at half maximum (FWHM), A is the integrated area for a one-dimensional cut through the data, and $\vec{q}_0$ is the peak position or the maximum of SRO diffuse scattering (normally close to the superlattice peak position). The inverse of the FWHM can be used to evaluate the correlation length of SRO. Finally, the peak position is strongly affected by size-effect scattering. Size effect tends to shift the SRO peak away from the nominal position and lead to an asymmetric profile around the superlattice peak positions.

Simultaneous fits of the SRO, size-effect, and TDS contributions to the diffuse scattering were made for each of the line scans. Figure 6 shows an example of the fitting of both slow-cooled and quenched $Fe_{82.3}Ga_{17.7}$ along $[1LL]$ direction in reciprocal space. The different hatched areas indicate the different contributions of size-effect, TDS, and SRO scatterings to the total intensity.

V. DISCUSSION

A. SRO or LRO

After fitting the data, information about systematic evolution of the peak width, area, and position for SRO peaks is obtained. The peak width can also be discussed in terms of the correlation length, defined as $\frac{1}{w}(a)$, where a is the lattice constant in real space. The correlation length represents the average size of the SRO clusters. Figure 7(a) shows the evolution of the correlation length as a function of concentration and heat treatment along different crystallographic directions based on (0.5 0.5 0.5) and (100) peaks.

The plot indicates that the correlation length increases with Ga concentration for both quenched and slow-cooled samples, corresponding to the expected growth of Ga clus-
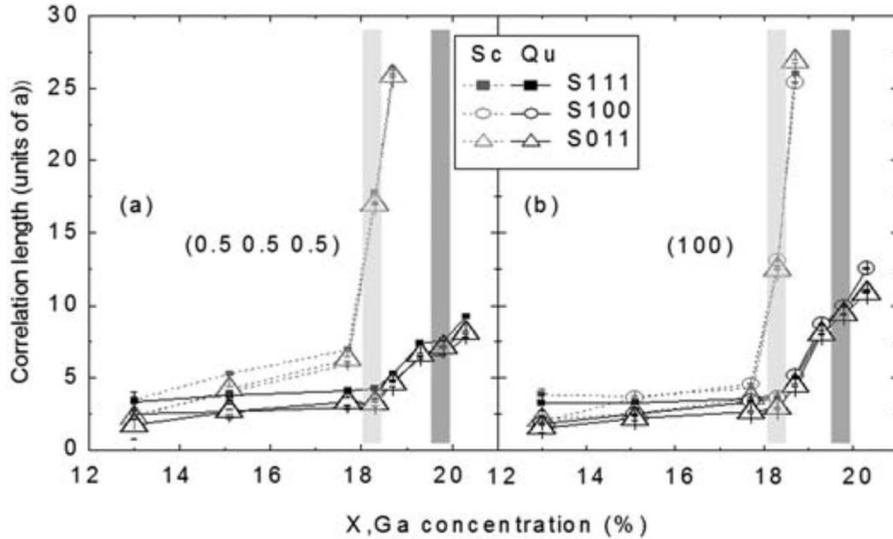
FIG. 7. Correlation lengths of Ga SRO versus Ga concentration for different heat treatments as determined from the widths of (0.5 0.5 0.5) and (100) SRO peaks cut in different crystallographic directions. Dashed and gray lines stand for slow-cooled (Sc) results while solid and black lines stand for quenched (Qu) results. The three symbols "■," "○," and "△" indicate the three cut directions of (111), (100), and (011), respectively. The shaded vertical rectangles indicate the Ga composition where MS reaches first maximum for both slow-cooled (~18–18.5 at. %, lighter gray) and quenched samples (~19.5–20 at. %, darker gray).

ters with the addition of Ga. In the slow-cooled samples, the correlation length experiences a sharp increase occurring close to the MS maximum around 18 at. % Ga. This indicates that SRO cluster sizes larger than 3–5 nm are detrimental to MS. The tendency for LRO to suppress MS in slow-cooled alloys with Ga concentrations larger than 18.7 at. % has also been noted from TEM studies.[7] Our results indicate that fairly small clusters are sufficient to suppress MS, rather than a requirement of true LRO.

The situation is somewhat different with the quenched samples. As shown in Fig. 1, quenching extended the enhanced MS to higher Ga concentrations when compared to slow-cooled samples. For the quenched samples, Ga clusters also increase in size near 18 at. %, however the clusters do not grow as quickly with concentration as compared to the slow-cooled samples. The smaller cluster size in quenched samples likely results from the retention of thermal disorder in the alloy structure during the quenching process. In the quenched samples, we also note that maximum MS occurs when the SRO reach 2–3 nm average size.

B. Shapes of SRO regions

From Fig. 7, the correlation lengths of SRO along different crystallographic directions for the same sample could be compared. When the Ga concentration is less than 18 at. %, the correlation length of SRO peak is slightly larger along the [111] direction in comparison to that along either the [011] or [100] directions. So, for low Ga concentrations, there is a small tendency for elongated clusters along the [111] direction. When Ga concentration is larger than 18 at. %, the correlation lengths of the SRO clusters become the same along different direction, indicating that the larger SRO clusters are isotropic and spherical in shape.

C. Size effect

Figure 8 shows the fitted peak position of both (0.5 0.5 0.5) and (100) SRO peaks. At lower concentrations, the peak

positions are strongly shifted from the nominal superlattice positions. The shift of the peak intensity and the general asymmetry of the peakshape [most notably the (100) peak shown in Figs. 4(c) and 4(e)] indicate the influence of size-effect scattering.[18] In formulas (3) and (4), as mentioned before, β has the same sign as $(f_{Ga} - f_{Fe})$. In x-ray scattering experiment, f_{Ga} is larger than f_{Fe}, hence β is positive. In formula (3), the first term is symmetric at $L=0.5$ while the second term increases at $L=0.5$. In formula (4), the first term increases at $H=1$. Hence both of the peaks are shifted to the higher-q side of the nominal superlattice peak position and the size-effect scattering contributes an asymmetric intensity at the superlattice position. On the other hand, the shift of (100) peaks is mainly from the first term while that of (0.5 0.5 0.5) peaks is mainly from the second term in formulas
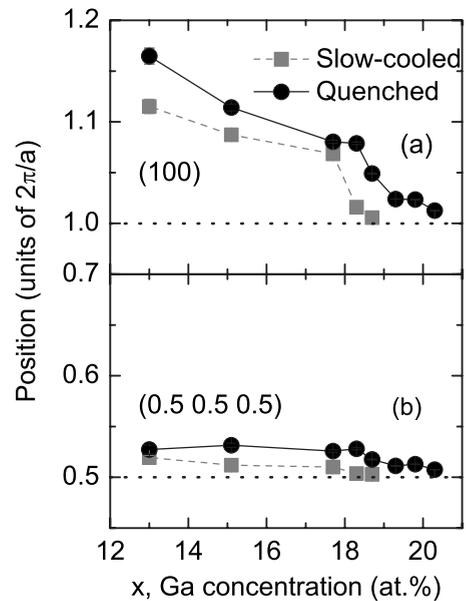

FIG. 8. Positions of (100) peaks (a) along (100) direction and positions of (0.5 0.5 0.5) and (b) peaks along (111) direction as a function of Ga concentration.
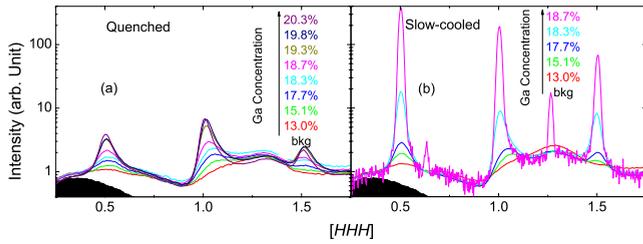
FIG. 9. (Color online) The normalized intensity along the $[HHH]$ direction for (a) quenched and (b) slow-cooled samples, respectively, for various Ga concentrations. The black region is background.

(1), (3), and (4). It is observed that the shift of (100) peak is more notable. From this we surmise that in formulas (1), (3), and (4), the terms with lower index of β (nearest neighbors) are more dominant. However, we are not able to fully describe the large peak shift based on the simplified formulas used. Figure 8 shows that the SRO peaks return to the nominal positions with symmetric peak shapes beyond 18 at. % Ga concentration. Similar observation was reported for slow-cooled $Fe_{81.6}Ga_{18.4}$ by Huang *et al.*[19] This behavior is expected and can be explained by reduction in size-effect scattering due to the formation of large clusters. In the large clusters, the Ga distribution within a cluster is similar to the LRO structure and hence the local structure is more symmetric. This symmetry will reduce the positional distortions of the atoms resulting in the reduction in the size-effect scattering.

The influence of size effect can also be observed by neutron scattering.[11] It was reported that the (100) and (300) peaks are shifted to lower q, which was different from the result of x-ray diffuse scattering. This observation from the comparison of the x-ray and neutron data gives convincing proof that size-effect scattering is the origin of the peak shift. In neutron scattering, the sign of $(f_{Ga}-f_{Fe})$ is opposite to our x-ray experiment due to the fact that the neutron-scattering length of Fe is larger than Ga.

D. Short-range ordered structure

In general, any quantitative description of the local structure of the SRO (in terms of Warren-Cowley short-range order parameters, for example), requires Fourier analysis of the diffuse-scattering data throughout the full reciprocal space. However, some information about the structure can be obtained from the line scans. Figure 9 shows a line scan along the [111] direction. This scan direction is useful since it contains both (0.5 0.5 0.5)-type positions expected only for $D0_3$ order and (111)-type positions that describe both B2 and $D0_3$ order (see Table I). Both (111) and (0.5 0.5 0.5) diffuse peaks appear for all Ga concentrations (as low as 13 at. %) for both quenched and slow-cooled samples. This provides good evidence of the importance of the $D0_3$-type Ga correlations in the clusters. This is perhaps not surprising, as LRO $D0_3$ phase is observed at slightly higher concentrations in the metastable phase diagram (Fig. 2).

We can refine the discussion of the atomic arrangement within the cluster by comparing the peak intensities observed
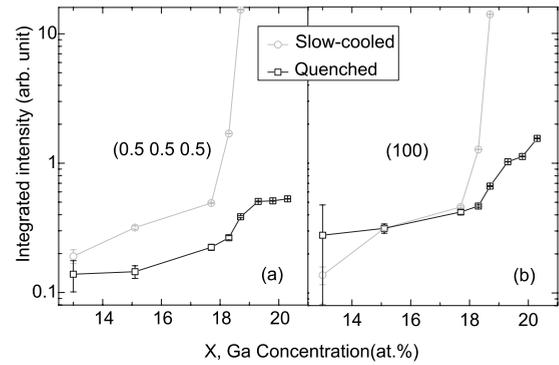

FIG. 10. Integrated intensity of Ga SRO peaks at (a) (0.5 0.5 0.5) and (b) (100) superlattice positions measured along (111) direction versus Ga concentration for the two different heat treatments.

along the [111] direction to those expected from LRO B2 or $D0_3$ structures. For the B2 structure, superlattice peaks are expected only at odd-integer positions along [111]. For $D0_3$ long-range order, all half-integer and odd-integer superlattice positions along the [111] direction are allowed. The measured intensity of such superlattice peaks is proportional to a product of the structure factor, Lorentz-polarization factor, and x-ray atomic form factors.

The Lorentz factor is given by $\frac{1+\cos^2(2\theta)}{2\sin(\theta)}$. Since the value of θ in our experiment is very small, Lorentz factor is roughly equal to $\frac{1}{\theta}$. Furthermore, we know in binary systems, the intensities of superlattice peaks are directly proportional to $(f_{Fe}-f_{Ga})^2$ and the x-ray form factor decreases with increasing $|\vec{q}|$. Hence for $D0_3$ ordering, superlattice peaks will appear at all half integer and integer positions along (111) and the intensity will decrease with increasing $|\vec{q}|$. This trend is observed in slow-cooled concentrations in Fig. 9 and we conclude that SRO in the slow-cooled alloys has $D0_3$-like local structure. The quenched concentrations exhibit a different trend in intensity. In general, the (111) peak is more intense than either the (0.5 0.5 0.5) or (1.5 1.5 1.5) peaks. This is unlike the slow-cooled samples and not expected for $D0_3$-type SRO, as explained above. Rather, the results suggest that clusters in the quenched alloys have some B2 character in addition to D03.

The difference in $D0_3$ and B2 structures can easily explain the variation in the atomic arrangements of clusters in the slow-cooled and quenched alloys. In the Fe-Ga system, Ga atoms repel one another. In slow-cooled samples, the Ga atoms have enough time and thermal energy to move themselves as far as possible, resulting in the $D0_3$ structure where the first Ga-Ga coordination shell occurs at the third nearest-neighbor position. In quenched samples, high-temperature thermal disorder is frozen in and Ga pairs can be found in the second coordination shell (i.e., at the body-centered positions), corresponding to B2 structure. The metastable phase diagram shown in Fig. 2 indicates that the ordering into the B2 structure is expected at higher temperatures and plays a larger role in the cluster formation of the quenched samples, especially at higher concentrations. This is also supported by Fig. 10, in which the integrated intensities of (0.5 0.5 0.5) peaks are notably smaller than that of (100) peaks for large

Ga concentration. This indicates that B2-like Ga pairing is much more prevalent at the highest Ga concentrations in the quenched samples since (0.5 0.5 0.5)-type superlattice peaks are not allowed for B2 ordering.

E. Relation between MS and SRO in Fe-Ga alloys

The relation between large MS and the alloy structure is an open question that has been discussed from extremely different perspectives. One model[4,5] uses strong coupling between the underlying A2 matrix and tetragonal $D0_3$-like precipitates to explain MS. In this model, $D0_3$ precipitates transform into strongly distorted face-centered tetragonal (fct) islands. The size of the fct strains is thought to control MS. Due to exchange coupling between fct precipitates and A2 matrix, the application of magnetic field to the multidomain structure will line up the tetragonal axes, leading to large MS strain. In principle, such tetragonal domains should be clearly visible in the x-ray scattering measurements as diffuse scattering with clear shift or split in superlattice peak due to tetragonal strain. However, based on our results, there is no evidence to support the existence of this tetragonal structure since we did not observe any splitting even on the sharpest superlattice peaks observed in slow-cooled compositions. This is in apparent conflict with observations of peak splitting in the neutron data from slow-cooled Fe-Ga alloys by Cao *et al.*[11] The diffuse peaks are observed to shift from the nominal superlattice positions to the positive-q side of (H00), clearly indicating that the shifting is due to atomic size effect. This fact has been reenforced by recent resonant x-ray diffraction. In that experiment, we chose different incident energies close to the K edges of Fe and Ga such that the sign of ($f_{Ga} - f_{Fe}$) was changed. The results showed that the SRO peaks shifted to either higher q or lower q relative to nominal position.[20]

Another proposed model relates the large MS to Ga pairing found in the B2 atomic structure.[2,3] Band-structure calculations performed using the full-potential linearized augmented plane wave determined the magnetostrictive coefficient for different Ga ordering patterns. Calculations predict that the B2 structure contributes positively to MS while $D0_3$ structure will contribute negatively. The negative effect of the $D0_3$ structure appears to be accurate, as the appearance of large $D0_3$ SRO or $D0_3$ LRO, sharply decreases MS. However, rather small $D0_3$ SRO found at lower concentrations apparently have little or no effect on MS. From Fig. 1, it is observed that heat treatment has little (if any) influence on MS at concentrations below the first maximum. However, different heat treatments give rise to different SRO cluster sizes, negating any possible role of very small clusters. Furthermore in $Fe_{96}Ga_4$, no SRO is found

while an enhancement of magnetostriction is observed. Thus, in the lower concentrations, the enhanced MS arises primarily from shear softening combined with changes in the magnetoelastic coupling.

The role that the Ga pairing plays in enhancing MS is still unclear. At concentrations where MS of slow-cooled samples reaches the first maximum and quenched samples begin to possess larger MS, the appearance of B2-like contributions to the SRO implies a growing amount of Ga pairing. Based on the band-structure predictions, the increased Ga pairing should increase the MS. However, it does not appear that it is possible to retain a higher degree of pairing by thermal treatment beyond ∼20 at. % Ga for the first peak. Thus, the gain in MS from Ga pairing is at most 15 at. %. It is also possible that quenching simply delays $D0_3$ ordering, allowing additional growth of the MS coefficient.

VI. CONCLUSION

Transmission synchrotron x-ray diffraction was used to investigate the structure of Fe-Ga alloys. The evolution of SRO was studied as a function of Ga concentration and heat treatment to clarify the role of Ga ordering in the large MS along [100] direction.

No SRO was found in $Fe_{96}Ga_4$. Between 13 and 20.3 at. %, the $D0_3$-type SRO increases in size with Ga concentration eventually forming the LRO $D0_3$ structure. The size of $D0_3$ SRO is suppressed by quenching for the same concentration with clusters tending to become isotropic in shape as Ga concentration increases. These results push forward our understanding of the ordering processes in the Fe-Ga alloys; addition of Ga into Fe inevitably introduces SRO in the Fe-Ga solid solutions with Ga concentrations above certain amount. Nanoscale $D0_3$ clusters (>2–5 nm) and $D0_3$ LRO around the first MS maximum suppress MS dramatically. B2-like contributions to the SRO were observed only in quenched samples for large Ga concentration. However the relation of Ga pairing expected from the B2 contributions and enhanced MS is unclear.

*Present address: NIST Center for Neutron Research, NIST, Gaithersburg, Maryland 20899, USA.

[1] E. M. Summers, T. A. Lograsso, and M. Wun-Fogle, J. Mater. Sci. **42**, 9582 (2007).

[2] R. Wu, J. Appl. Phys. **91**, 7358 (2002).

[3] R. Wu, Z. Yang, and J. Hong, J. Phys.: Condens. Matter **15**, S587 (2003).

[4] A. G. Khachaturyan and D. Viehland, Metall. Mater. Trans. A **38A**, 2308 (2007).

[5] A. G. Khachaturyan and D. Viehland, Metall. Mater. Trans. A **38A**, 2317 (2007).

[6] C. Kittel, Rev. Mod. Phys. **21**, 541 (1949).

[7] Q. Xing, Y. Du, R. J. McQueeney, and T. A. Lograsso, Acta Mater. **56**, 4536 (2008).

[8] M. Wuttig, L. Dai, and J. Cullen, Appl. Phys. Lett. **80**, 1135 (2002).

[9] A. E. Clark, K. B. Hathaway, M. Wun-Fogle, J. B. Restorff, T. A. Lograsso, V. M. Keppens, G. Petculescu, and R. A. Taylor, J. Appl. Phys. **93**, 8621 (2003).

[10] O. Ikeda, R. Kainuma, I. Ohnuma, K. Fukamichi, and K. Ishida, J. Alloys Compd. **347**, 198 (2002).

[11] H. Cao, P. M. Gehring, C. P. Devreugd, J. A. Rodriguez-Rivera, J. Li, and D. Viehland, Phys. Rev. Lett. **102**, 127201 (2009).

[12] K. Perduta, J. Olszewski, S. Busbridge, and M. Nabialek, Acta Phys. Pol. A **114**, 1537 (2008).

[13] R. A. Dunlap, J. D. McGraw, and S. P. Farrell, J. Magn. Magn. Mater. **305**, 315 (2006).

[14] X. Zhao, N. Mellors, S. Kilcoyne, and D. Lord, J. Appl. Phys. **103**, 07B320 (2008).

[15] T. A. Lograsso and E. M. Summers, Mater. Sci. Eng., A **416**, 240 (2006).

[16] S. Datta, M. Huang, J. Raim, T. A. Lograsso, and A. B. Flatau, Mater. Sci. Eng., A **435-436**, 221 (2006).

[17] J. L. Zarestky, V. O. Garlea, T. A. Lograsso, D. L. Schlagel, and C. Stassis, Phys Rev B **72**, 180408(R) (2005).

[18] B. E. Warren, *X-Ray Diffraction* (Dover, New York, 1990).

[19] M. Huang and T. A. Lograsso, Appl. Phys. Lett. **95**, 171907 (2009).

[20] Y. Du, Y. Puzorov, M. Huang, G. E. Ice, and R. J. McQueeney (unpublished).